Wireless Actuation for Soft Electronics-free Robots

Jingxian Wang[1,2,3], Yiwen Song[1], Mason Zadan[1], Yuyi Shen[1],
Vanessa Chen[1], Carmel Majidi[1], Swarun Kumar[1]
[1]Carnegie Mellon University, [2]Microsoft Research, [3]National University of Singapore
[1,2]USA, [3]Singapore

ABSTRACT

This paper proposes a new primitive that allows soft robots to be physically controlled in a completely non-line-of-sight context using wireless energy – a process we call wireless actuation. Soft robots, which are composed entirely of soft materials and exclude any rigid components, are highly flexible platforms that can change their shape. This paper considers a specific class of soft robots composed of liquid-crystal elastomers (LCE) that are entirely electronics-free and engineered to change shape when heated to 60 °C. Traditionally, such robotic systems must be in line-of-sight of a light source, such as infrared to be moved, or require an external power supply for Joule heating and often take several tens of seconds to heat. We present WASER, a novel RF-based heating platform that allows electronics-free robots to be actuated rapidly (within a few seconds) and potentially in non-line-of-sight. WASER achieves this through innovations in both wireless systems and material science. On the wireless front, WASER develops a new blind beamforming solution that directs high-power wireless energy at fine spatial granularity without electronics on the robot to provide feedback. On the material science front, WASER exhibits heat-responsive shape-morphing and energy-harvesting material functionalities that allow for rapid wireless heating. We implement and evaluate WASER and demonstrate diverse shape-morphing capabilities.

CCS CONCEPTS

• **Computer systems organization** → **Robotics**; **Sensors and actuators**; • **Hardware** → **Beamforming**; **Emerging interfaces**; • **Networks** → **Cyber-physical networks**.

KEYWORDS

Wireless Actuation, Beamforming, Soft Materials

ACM Mobicom '23, October 2–6, 2023, Madrid, Spain

ACM ISBN 978-1-4503-9990-6/23/10.
https://doi.org/10.1145/3570361.3592494

ACM Reference Format:
Jingxian Wang[1,2,3], Yiwen Song[1], Mason Zadan[1], Yuyi Shen[1],, Vanessa Chen[1], Carmel Majidi[1], Swarun Kumar[1]. 2023. Wireless Actuation for Soft Electronics-free Robots. In *The 29th Annual International Conference on Mobile Computing and Networking (ACM MobiCom '23), October 2–6, 2023, Madrid, Spain.* ACM, New York, NY, USA, 16 pages. https://doi.org/10.1145/3570361.3592494

1 INTRODUCTION

In this paper, we introduce a framework for engineering soft robots that move and change shape in response to *wireless actuation*. State-of-the-art soft robots offer unique features compared to traditional robots: miniaturization [62], shape morphing [33], and adaptability to constrained terrains [25, 63]. While various classes of soft robots exist, we target the development of machines that are composed entirely of soft materials and exclude any rigid components such as integrated circuits or batteries [21, 50, 71]. To achieve this, we use liquid-crystal elastomers (LCE) [46, 60], a shape-memory polymer that has become increasingly popular in soft robotics [27]. Innovations in material science have shown that LCEs can exhibit complex and reversible shape changes upon *thermal* stimulation [34, 35, 70]. When heated to 60° Celsius [72], LCEs can undergo maximal contraction with strains and stresses comparable to that of natural skeletal muscle [14].

Unfortunately, existing approaches to actuate LCE-based soft robots remain rudimentary. Past work leverages Joule heating [7, 14, 20, 32] or Peltier heating [75] to produce heat through electrical current delivered by an external DC power supply. Researchers have also demonstrated LCE soft robots that can be heated by light sources such as infrared and ultraviolet [15, 24, 38, 39, 51, 61]. However, these systems require line of sight with the light source and are therefore not robust to obstacles or occlusions. While magnetic actuation [30] can move small-scale robots, the current methods are limited to a maximum distance of a few centimeters from the magnetic energy source. In general, existing LCE actuation solutions are constrained by their requirement for a tethered electrical connection to an external power supply, a limited actuation range, or line-of-sight positioning with a light source. Such constraints limit the deployment of LCE-based soft robots in real-world environments that require operating within confined and enclosed spaces.

To address this limitation with LCE-based soft robots, we present WASER (**W**ireless **A**ctuation for **S**oft **E**lectronics-free

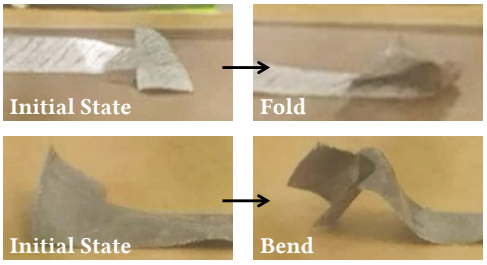

Figure 1: WASER precisely beams wireless energy to our thermally responsive soft robot to induce various shape changes (e.g., folding and bending).

Robots), the first wireless heating platform that enables high-resolution heating actuation for soft robots within a non-line-of-sight context. Specifically, we build a programmable high-power beamforming platform using off-the-shelf RF hardware. WASER induces the heat actuation of soft robots wirelessly by applying 2.4 GHz signals across an array of distributed antennas. The ultimate goal of WASER is to actuate the soft robot with speed and precision. For example, WASER aims to heat different parts (1-2 cm wide) of the robot body to enable various shaping changing and motion capabilities.

System Overview: WASER is developed through an interdisciplinary effort that brings together wireless systems and material science research. On the wireless front, WASER builds on beamforming technology, which focuses wireless energy towards a targeted area [68]. WASER generates optimized beamforming vectors that maximize wireless power to the desired area of the robot in the non-line-of-sight while avoiding rising temperature outside. On the materials front, we combine thin-film LCE with soft, mechanically compliant conductive layers. Together, these materials allow for electronics-free soft robots that harvest 2.4 GHz wireless energy and convert this stimulation into shape change. Our WASER soft robot achieves significantly improved thermal and electrical conductivity without detrimentally altering its mechanical or shape-morphing properties. A detailed experimental evaluation shows that our WASER heating platform achieves 17.8 mm heating resolution[1]. We show that WASER can actuate desired shape deformation of the robot (starting from room temperature) within 1.5 seconds using 20 W. Further, we demonstrate multiple modes of shape change that can be achieved with the WASER robot.

Our primary challenge in WASER's design is to precisely actuate the desired part of a soft robot. In other words, WASER needs to find the optimal beamforming vector applied across the antenna array to focus wireless energy on the desired areas of the soft robot while suppressing temperature rises outside the targeted area. Traditionally, we could infer the optimal beamforming vector by exchanging wireless channel information between the target and the beamforming platform. However, our target – an electronics-free soft robot – does not explicitly provide its channel feedback to our platform. Further, the soft robot is in the non-line-of-sight, so inferring the optimal beamforming vector of the robot becomes more challenging. To solve this problem, WASER designs creative alternatives to solicit indirect feedback of the robot, coupled with novel approaches to model signal propagation in the non-line-of-sight radio environment. Specifically, we estimate the channel of the WASER robot by deploying a grid of 2.45 GHz LED-equipped energy harvesters. A detailed description of designing the harvesters can be found in Sec. 5.4. The brightness of the distributed LEDs represents the wireless channel information around the soft robot at multiple known locations. Note that WASER assumes the relative positions of the distributed LED array to that of the soft robot is known before any actuation is applied. WASER then can interpolate the wireless channel of the soft robot based on the brightness of the LED array. Yet, the RF reflectors in the environment could generate multipath and influence the channel estimation of the robot. To address this challenge, WASER applies channel probing to estimate the radio environment. In effect, this allows WASER to derive the optimal beamforming vector that precisely beams to a particular body part of our robot. After estimating the channel, WASER further uses the LED array to monitor the robot's shape change and ensure a minimal microwave leakage preventing rising temperature outside the targeted area.

In addition, WASER must improve the speed of LCE-based soft robot actuation – i.e. reduce the heating time required for the robot to exhibit a maximized shape change for a reasonable total transmitted power. Previous work has shown that it takes 40 seconds to actuate an LCE-based soft robot with a hundred-Watt microwave power source [69]. This slow pace of actuation limits its application in LCE-based soft robotics. The reason for this inefficacy is that prior work uses dielectric heating which is not efficient to convert microwave signals into thermal energy within LCE polymers. Instead, WASER utilizes a novel material architecture and structure that combines highly conductive liquid metal alloy with the liquid-crystal composites. WASER then optimizes the geometry of soft robots so that it resonates well at 2.45 GHz. As a result, the robot can be heated based on both dielectric heating and induction heating which induces strong eddy current within the conductive component of the soft robot. Another challenge WASER must address is to avoid edge effects of the conductors in a strong EM field. The edge effects cause the electrons to concatenate on the edges and corners of the soft robot, which limits the shape changing capabilities of the soft robot. To address this problem, we design novel textural material structures for the robot. Sec. 6

[1]The heating resolution is defined as the distance that the energy density attenuates 3 dB from the peak (Sec. 8.6).

describes our design choices that improve the speed of actuation to exhibit the desired shape changes.

We build a prototype of a beamforming platform for actuating soft robots. Our prototype uses four USRPs paired with solid state amplifiers. Our experiments show that WASER can heat the soft robot from 20°C to 60°C within 5 seconds using a 2.5 W total transmit power. A detailed experimental evaluation on WASER shows that the heating platform achieves a high-precision heat distribution with an average spatial resolution of 17.8 mm. We also demonstrate shape morphing capabilities enabled by WASER which we describe in Sec. 8.7.

Potential Applications: We envision the WASER actuation platform that can function as an open-source tool available for broad uses by researchers in wireless, soft robotics, and material science in areas including smart manufacturing, food processing and machine maintenance. Indeed, we see WASER as a primitive that enables many applications, some of which we elaborate on in Sec. 9.

Safety: We limit the maximum transmit power of WASER to 20 Watts (43 dBm) which is the typical transmit power of a 4G cellular antenna [6]. WASER operates at 2.4 GHz whose wireless power reduces by about 40 dB in the first meter [41]. Thus, the power level beyond 1 meter is safe for general public exposure. To guarantee the safety and avoid jamming the existing Wi-Fi devices, we deploy our system in a flexible Faraday shield. The actuation range is constrained by the size of the shield. We describe more details about the Faraday shield and possible methods to reduce the transmit power in Sec. 7 and Sec. 9 respectively.

2 RELATED WORK

Electronics-free Soft Robots: Inspired by nature, soft-bodied robots that exclude any rigid components have the potential to exhibit unprecedented adaptation to harsh or uncertain environments [54] and achieve motions such as twisting, bending, and folding. In addition, removing rigid components such as batteries or integrated circuits offers a promising path to robot miniaturization [26, 52] and thus helps the soft robot operate in confined spaces [65]. Prior work has performed actuation using light sources requiring line-of-sight positioning to the electronics-free robot [24, 51, 61]. In fact, recent research efforts have shown to actuate magnetic electronics-free microrobots (with a width of less than 1 cm) in non-line-of-sight environments using near-field coupling coils [30] or magnet-composed gearing systems [22]. However, these methods are limited to a maximum range of 4 cm in proximity to the coil. Further, as magnetic control works in the low frequency domain, it is not capable of providing partial actuation when the soft robot is of centimeter size. In contrast, WASER builds a microwave-based actuation platform for electronics-free soft robots that simplifies precise energy delivery in confined spaces and non-line-of-sight environment. This platform aims to develop robotic systems that can enter hibernation for a long period of time and reactivate when beamed energy is applied without the need to change batteries or retrieve the system for charging or maintenance when in hard-to-reach locations.

Thermally Responsive Soft Robot Actuation: Our study explores controlling soft materials that exhibit complex shape changes upon thermal stimulation. We specifically focus on LCE due to its popularity in soft robotics and versatility in manufacturing, shape programmability, and device-level integration [27]. Past efforts with LCE in soft robotics typically relied on Joule heating to induce heat and shape change. This is accomplished by embedding the LCE with resistive materials [7, 14, 20, 66]. However, this method requires a wired connection to an external power supply, which continuously provides current flowing through the resistive elements. This dependency on a tethered connection to external hardware significantly limits the mobility of robotic systems. Recently, optic-based actuation methods have been explored using scanning lasers [51], ultraviolet [15], and even infrared lights [76]. However, these constrain the operation space of the robot to be within line-of-sight of the light emitters.

More recent work [69] proposes using high-power microwave signals at 2.4 GHz to actuate LCE in non-line-of-sight (NLoS), but blasts microwave energy blindly and fails to precisely and rapidly actuate the LCE (i.e., it takes 40 seconds to actuate the robot). In contrast, WASER strives to improve the precision and speed of actuating the thermally responsive soft robots in NLoS by developing a microwave beamforming actuation platform.

Wireless Power & Beamforming Systems: Key to enabling wireless heating is accurately delivering wireless power. Prior work [9, 55, 56] has built wireless power delivery and charging systems using cavity resonators and rotational mechanical systems [31]. While past solutions focus on simultaneously delivering sufficient power to nearly any location in a large chamber, WASER develops a beamforming system to precisely deliver the wireless power at desired parts of a soft robot while suppressing temperature rises outside the targeted area.

Beamforming techniques [36, 49, 64] have been widely explored in wireless networking research. Today, we actively use beamforming techniques in 5G and Wi-Fi to improve the network throughput to accommodate the fast-growing demand of wireless services [2, 53]. Beamforming traditionally requires the sender and the receiver to exchange channel information so that they can better direct the wireless energy

towards each other. However, in our context, the soft robot – the recipient of beamformed energy – is electronics-free, motivating the need for new beamforming solutions.

Prior work has explored beamforming systems to power battery-free wireless devices whose wireless channels are unknown, such as RFID [40, 68] and NFC tags [67]. However, in these contexts, the tags only require about 50 uW to be activated which is 200000× lower than the power required to actuate the battery-free soft robots. In addition, the tags can communicate channel feedback with the senders once they are successfully activated. Some customized tags are able to communicate 1-bit phase feedbacks with the sender [13]. In contrast, our electronics-free robots do not have the capability to communicate with the beamforming system. Hence, WASER must design a high-power beamforming system without any active feedback from the electronics-free robots.

3 PRIMER ON MICROWAVE HEATING

Over the past decade, researchers in the wireless community have widely explored the capabilities of 2.4 GHz unlicensed frequencies for networking and sensing. Historically, however, the ISM (Industrial, Scientific and Medical) band was initially allocated primarily for non-communication purposes, such as microwave heating. This section describes the applications and mechanism of microwave heating.

3.1 Applications of Microwave Heating

One of the most commonly used microwave heating devices is the domestic microwave oven. The microwave oven cooks food by blasting wireless power (between 0.5 kW and 2 kW) at a center frequency of 2.45 GHz. Industrial scale heating is another major sector where microwave heating techniques are deployed, say for plastic softening [1], drying [47], and tempering deep frozen meats [48]. In addition to industrial manufacturing and food processing, microwave heating has also been used to perform sterilization, such as sterilizing dental instruments [74] and N95 respirators [16]. Industrial microwave systems either use 2.45 GHz or 915 MHz wireless signals within the transmitted power range of 3 kW and 120 kW. Recent work has also used microwave heating to facilitate chemical reactions [10]. The benefits of applying microwave heating are that they enable deep internal heating and offer a significant reduction in heating time.

3.2 Mechanisms of Microwave Heating

When wireless signals interact with an object, a part of the electromagnetic energy is absorbed and converted into thermal energy or heat. The conversion can be attributed to either dielectric loss or conductive loss, leading respectively to dielectric or induction heating. The relative contributions of both heating mechanisms to an object are heavily dependent on the underlying materials of that object. We describe the details of each microwave heating mechanism below:

Dielectric Heating: For dielectric materials or electrical insulators such as pure water, there is little free charge inside. However, rapidly changing electric fields (e.g., 2.4 GHz EM signals) can cause polarization and generate heat within the material. This is because the molecular dipoles inside the material are rendered polarized, i.e., each molecular dipole (e.g., a water molecule) has one end carrying positive charges and the other end carrying negative charges. Note that a molecular dipole is always aligned with the direction of an external electric field. Thus, a rapidly oscillating EM field causes the molecules inside dielectric materials to rotate rapidly, aligning themselves with the external electric fields. When molecules rotate, the collisions among them dissipate energy and contribute to heating. The dielectric loss is governed by the relative permittivity and the loss tangent of the underlying material [23]. Dielectric heating is the main cause of heating when we cook food in a microwave oven.

Induction Heating: Also known as eddy current heating, induction heating is the dominant heat contributor for conductive materials. Since there are a large number of free electrons in conductors, a rapidly changing magnetic field will induce currents inside a conductor [17] following Faraday's Law. The induced current generates heat according to Joule's First Law. In addition to this, the oscillating magnetic field will contribute to hysteresis losses if the underlying materials have high values of loss tangent and permeability, which generates heat as the magnetic moments within materials try to oppose the rapidly changing magnetic field.

Microwave heating of real-world materials is usually a combination of the two heating mechanisms above. LCE barely consists of any free electrons, so it is heated dominantly due to dielectric heating. Meanwhile, the reason that conductive objects can heat extremely fast in a microwave oven owes to induced eddy currents. WASER strives to use both heating mechanisms to rapidly and precisely control the soft robot, both through a careful choice of robotic materials and our beamforming system design.

4 BRIEF OVERVIEW

Fig. 2 summarizes the setup of our system. Our objective is to design a soft robotic platform that can precisely heat the soft robot at fine spatial granularity and achieve this heating within a few seconds from an external wireless energy source. We assume that the robot could potentially be in non-line-of-sight. We assume that the entire system is enclosed within an RF shield or enclosure that prevents microwave leakage to ensure safety. We further assume that the location of the soft robot is known and that it is designed to move predictably

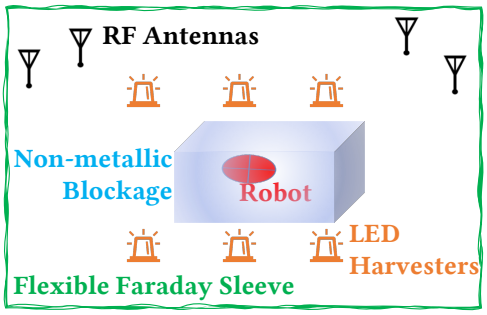

Figure 2: The soft robot can be in non-line-of-sight (NLoS) due to blockages. WASER estimates the channel at the soft robot using battery-free LED harvesters distributed outside the blockage. WASER can actuate the soft robot with 2.5 W which is a typical transmission power of a Wi-Fi repeater [4]. To ensure safety, the entire system is enclosed by a flexible Faraday sleeve illustrated by the green line. Sec. 7 describes the actual deployment of the system.

when heated to specific temperatures. We assume access to at least some locations within the Faraday shield that are in line-of-sight of our system to place LED harvesters. We note that as shown in Fig. 2, the harvesters can potentially entirely be outside the non-metallic enclosed space where the soft robot is located. Since the enclosed space is metallic, WASER re-uses it as the RF shield and the LED harvesters would need to be placed within the enclosed space.

The rest of this paper addresses two key design questions of WASER: (1) First, we develop a high-power beamforming solution at our wireless energy source that efficiently heats the desired points on the robot, without requiring electronics physically attached to the robot (Sec. 5); (2) Second, we present the design of the soft robotic platform's material that allows it to remain flexible while conducting heat effectively (Sec. 6). We conclude with detailed system implementation and evaluation (Sec. 7-8).

5 HIGH-POWER BLIND BEAMFORMING

LCE-based soft robots can be remotely actuated through the application of wireless heating. However, wireless channel feedback from the soft robots is unavailable, meaning that it is challenging to accurately actuate the desired spots of them via beamforming. The situation gets even worse when the robot operates in non-line-of-sight. To address this challenge, we introduce a high-power *blind* beamforming algorithm[2] that can precisely actuate the soft robot without any response of the robot. Specifically, WASER achieves this by (1) acquiring accurate estimates of channel information indirectly from multiple locations using LED-equipped energy harvesters surrounding the robot (potentially at a visible place); (2) interpolating the channel distribution to estimate the wireless channel at the robot.

5.1 Problem Formulation

Our goal is to perform accurate beamforming towards the robot, even focusing on individual sub-sections of the robot body. As a result, WASER must infer the wireless channel state information at different parts of the soft robot.

We now mathematically characterize the relationship between wireless channels and beamforming weights in the soft robotic context. We represent the channel at a desired point on the soft robot by a complex vector $\mathbf{h} \in \mathbb{C}^N$, where N is the number of antennas. The n-th element of $\mathbf{h}$, denoted by $\mathbf{h}_n$, then represents the channel observed by the n-th antenna. $|\mathbf{h}_n|$ denotes the channel strength observed by the antenna n, and $\angle\mathbf{h}_n$ refers to the phase of the wireless channel between the n-th antenna and the robot. We use $\mathbf{w} \in \mathbb{C}^N$ to denote the beamforming vector applied to the N transmitting antennas. In order to beam maximum wireless energy to the robot, WASER must find out the optimal $\mathbf{w}$:

$$\max_{\mathbf{w}} \quad \left|\mathbf{w}^\top \mathbf{h}\right| \tag{1}$$

$$\text{s.t.} \quad |\mathbf{w}|^2 \leq P \tag{2}$$

where Eqn. 2 restricts the total transmitting power P from all distributed antennas. Given an observed wireless channel $\mathbf{h}$, the solution to the optimization Eqn. 1 can be derived as

$$\mathbf{w_o} = \sqrt{P}\frac{\bar{\mathbf{h}}}{|\mathbf{h}|} \tag{3}$$

where $\mathbf{w_o}$ is the optimal beamforming vector that beams maximized wireless energy to the robot and $\bar{\mathbf{h}}$ is the complex conjugate of $\mathbf{h}$. Ideally, the wireless channel information $\mathbf{h}$ between the soft robot and the distributed antennas can be measured by sending a known series of signals from the specific point on the soft robot. However, LCE-based soft robots are electronics-free and so cannot send any feedback.

5.2 Low-power Channel Probing

Since LCE-based soft robots are electronics-free, WASER must infer the channel of the soft robot indirectly. To address this challenge, our key approach is to deploy LED-equipped energy harvesters at known locations outside of any blockage that surrounds the robot shown in Fig. 2. WASER then estimates the wireless channel at each location where these energy harvesters are deployed, by measuring the brightness of the LED-equipped RF energy harvesters (Sec. 5.4).

Specifically, we design a channel probing algorithm using LED harvesters with 2.4 GHz signals. The challenge however is that the brightness of LEDs only shows the amplitude of

[2]Blind due to the absence of direct feedback from the robot.

the channel. In other words, we cannot directly measure the phase of the wireless channel. Thus, WASER must solve the *phase retrieval* problem. At a high level, WASER solves it by probing the LED harvesters with multiple beamforming vectors $\mathbf{W}_k$ where k represents the k-th probe. WASER finds the wireless channels of LED harvesters $\mathbf{h}$ by solving:

$$\min_{\mathbf{h}} \quad ||\left|\mathbf{W}^\top \mathbf{h}\right| - \mathbf{b}||_2^2 \tag{4}$$

where $\mathbf{W} = [\mathbf{W}_1, \mathbf{W}_2, \cdots, \mathbf{W}_K]$, and $\mathbf{b}_1, \mathbf{b}_2, \cdots, \mathbf{b}_K \in \mathbb{R}$ are measured amplitude of the LED harvesters for each probe. Given that the radio environment of WASER is multipath-rich, we adapt PhaseLift [8] to retrieve the phase and solve Eqn. 4. The algorithm [8] is guaranteed to converge when we apply $4 \times N$ times of channel probes, where N is the number of antennas. In our experiments, we deploy 4 antennas and apply 16 channel probing to infer the LED array's wireless channels. The computation latency to solve Eqn. 4 takes less than 1 second using devices described in Sec. 7.

5.3 Finding the Beamforming Vector

At this point, WASER can acquire wireless channel estimates at multiple locations around the robot. Now, WASER must estimate the channel of the robot, potentially in non-line-of-sight, and then use the channel information to find the optimal beamforming vector to beam maximized power to the robot. WASER achieves this by interpolating the channel estimates of the distributed harvesters obtained in Sec. 5.2.

Interpolating Channel Information: In compliance with FCC regulations, our high-power beamforming actuation is performed inside an RF shielded space (e.g., a Faraday sleeve) to prevent microwave leakage. The shielded space can be seen as a cavity resonator where EM signals form standing waves [18]. Thus, the x, y, z partitions of the electric field and magnetic field can be represented by a sinusoid product of the coordinates. We then use the Poynting's theorem to model the power distribution inside the cavity resonator with a combination of sinusoidal waves. Therefore, the power density S is as follows:

$$S(x, y, z) = C^2 \left[\sin^2\left(\frac{\pi x}{a}\right) \sin^2\left(\frac{\pi y}{b}\right) \sin^2\left(\frac{\pi z}{l}\right) \right] \tag{5}$$

where C, a, b, l are all constants. We then leverage the wireless channel $\mathbf{h}$ at each LED harvester's location (x_p, y_p, z_p) to solve the following optimization problem and interpolate the channels at the remaining locations:

$$\min_{C_n, a_n, b_n, l_n} \quad \sum_p \left| S(x_p, y_p, z_p) - \left|\mathbf{h}_n(x_p, y_p, z_p)\right| \right|^2 \tag{6}$$

this optimization is locally convex and can be solved by gradient descent. The interpolated channel of the antenna n at the desired position (x, y, z) would be $\left|\hat{\mathbf{h}}_n(x, y, z)\right| = S(x, y, z)$.

Similarly, we estimate the channel phase by linearly interpolating the phase of $\mathbf{h}_n(x_p, y_p, z_p)$ at the LED locations. Algorithm 1 summarizes our overall approach. This algorithm interpolates the optimal beamforming vectors for each point within the cavity regardless of the location of the soft robot. Note that WASER assumes that the location of the soft robot itself is known although its shape may change (see the section below on how we sense shape changes), this allows us to infer the optimal beamforming vector efficiently.

Detecting Continuous Shape Change: WASER can continuously detect the robot's shape change when it is actuated. The key idea is to leverage the LED-equipped energy harvesters and monitor their brightness when the soft robot is actuated. We evaluate WASER's capability to distinguish shape changes in Sec. 8.7. By detecting the shape change, WASER forms a closed loop to apply multiple beamforming vectors consecutively and induce a series of shape changes.

Algorithm 1 WASER Algorithm

$\mathbf{W}_1, \cdots, \mathbf{W}_K \leftarrow$ Randomly Initialized Beamforming Weights

for $k = 1$ to K **do**
  Beamform using $\mathbf{W}_k$, record the brightness of LEDs $L_1^{(k)}, L_2^{(k)}, \cdots, L_M^{(k)}$
Use PhaseLift to solve $\mathbf{h}^{(1)}, \mathbf{h}^{(2)}, \cdots, \mathbf{h}^{(M)}$
for $n = 1$ to N **do**
  Use interpolation to find C_n, a_n, b_n, l_n according to $\mathbf{h}_n^{(1)}, \mathbf{h}_n^{(2)}, \cdots, \mathbf{h}_n^{(M)}$
Loop:
Detect of shape change of soft robot
Use C_n, a_n, b_n, l_n to find $\mathbf{h}(x, y, z)$
Beamform using $\mathbf{w_o} = P\frac{\bar{\mathbf{h}}}{|\mathbf{h}|}$
end

5.4 Design of 2.4 GHz LED Harvesters

Why LED Harvesters?: At first glance, one may choose to interpolate the channel of the soft robot by deploying an array of 2.4 GHz backscatter devices that modulate the channel information onto their reflected RF signals at 2.4 GHz. WASER relies on those channel information to infer the channel of the soft robot, detect the shape changes of the soft robot, and prevent rising high-energy spots outside the targeted area. However, the wireless signals reflected back from 2.4 GHz backscatter could be overwhelmed by the high-power 2.4 GHz signals transmitting from our actuation platform. This causes interference and requires an additional expensive RF receiving unit to handle high-power received signals so that it can process the RF signals from 2.4 GHz backscatter. Instead, WASER uses LED-equipped energy harvesters to measure the wireless channel at 2.4

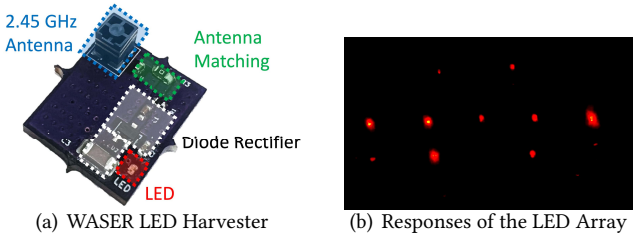

(a) WASER LED Harvester (b) Responses of the LED Array

Figure 3: WASER's Battery-free LED Harvesters.

GHz based on the brightness of the LEDs which can be read using a low-cost camera. By measuring the wireless channel through visible light responses rather than RF signals, our system functions even if the beamforming actuation platform is actively transmitting high-power wireless signals.

Designing LED Harvesters: To obtain visible light-based feedback, WASER uses a wireless energy harvester equipped with an ultra-compact low-power LED. Off-the-shelf components are chosen to keep cost and size down. Fig. 3 (a) describes the main components of our LED harvester. WASER harvesters absorb 2.45 GHz energy using an omni-directional chip antenna [43] that only have a dimension of 3 mm × 3 mm × 4 mm each. We place an LC impedance circuit to match our antenna to resonate well at 2.4 GHz. Received wireless power is rectified using a BAT15-04 Schottky diode pair to charge a ceramic supercapacitor. The ultra-compact LED is connected to the supercapacitor, so that the brightness of the LED directly captures how much wireless power the harvester absorbs. We use red LEDs over other colors, since the power consumption of red LEDs is lower at the same luminous intensity [57]. Fig. 3 (b) shows the LED responses. The brightness is linear with the voltage harvested [57]. Note that our LED harvesters have a threshold of received signal power > 11 dBm to respond.

6 ELECTRONICS-FREE SOFT ROBOTS

While our accurate high-power beamforming algorithm in Sec. 5 is one approach to efficiently heat the robot, its actual material architecture also plays an equally pivotal role. To see why this is important, note that prior work [69] takes around 40 seconds to actuate an LCE-based soft robot using an 800 Watt maximum transmit power at 2.4 GHz. In contrast, to ensure safety, WASER limits itself to a 20 Watt maximum transmit power. This section describes how: (1) WASER introduces novel material structures to significantly enhance actuation speed; (2) WASER consists of materials and fabrication methods that ensure the soft robot's mechanical compliance and deformability.

6.1 Structural Design of Soft Robots

Coating Shape-Morphing Polymer with Liquid Metal: LCE is a dielectric material, in which the energy conversion

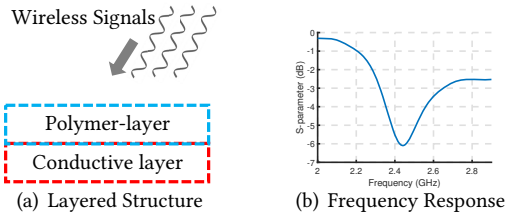

(a) Layered Structure (b) Frequency Response

Figure 4: (a) The cross-section of the WASER soft robot's layered material structure, which is composed of two layers: a polymer layer and a conductive layer (see details in Sec. 6.2). 2.4 GHz wireless signals can induce dielectric and induction heating for the polymer and conductive layer respectively. Note that wireless signals at 2.4 GHz can penetrate through dielectric materials such as LCE. (b) The S11 frequency response of our soft robot design simulated by CST Studio.

is only attributed to the dielectric losses. WASER utilizes a novel material architecture that combines LCE materials with a highly conductive alloy and can be patterned into a thin film. The key idea is to leverage both dielectric heating and induction heating mechanisms when the 2.4 GHz signals are applied to the soft robot. Specifically, a thin layer of a liquid metal composite is applied to the soft robot shown in Fig. 4 (a). We described details about the material of the liquid metal layer in Sec. 6.2. This layer induces induction heating that also transfers to LCE materials – allowing for rapid shape changes to the soft robot.

Optimizing the Geometry of the Soft Robot: Similar to designing a commercial Wi-Fi antenna, WASER must carefully design the geometry of the liquid metal composites so that they resonate well at 2.4 GHz. To do this, WASER uses an empirical approach where we test various geometries and simulate their resonance at 2.45 GHz. Fig. 4 (b) plots the frequency response of a robot design. Then we build the prototypes to test the performance (e.g., temperature distribution) using our beamforming platform. Our approach shows that a planar design with a thickness of 50 microns for the polymer layer and 5 microns for the liquid metal layer optimizes the heating performance.

Combating Edge Effects of the Conductive Layer: Microwave energy can raise the temperature of the conductive layer at ultra-low latency due to induced eddy currents. However, a flip side of the eddy current is that the electric field drives the electrons to edges of the conductor (e.g. in Fig. 5 (b)) [11], leading to these regions being disproportionately heated. Fig. 5 (c) shows a heat distribution of a *uniformly distributed* liquid metal composite (shown in Fig. 5 (a)) when 2.4 GHz wireless energy is applied. We notice that only the edges and corners are heated to a high temperature, which significantly distorts the heat distribution on the soft robot

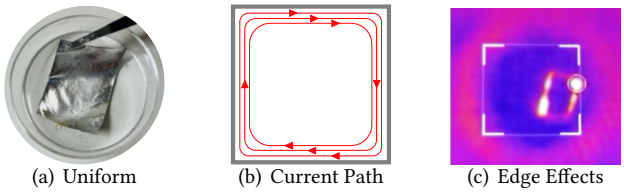

(a) Uniform (b) Current Path (c) Edge Effects

Figure 5: (a) A rectangular sample with uniformly distributed liquid metal. (b) Red lines show the path of induced eddy currents on the sample. (c) Heat distribution captured by a thermal camera. The brighter color shows a higher temperature.

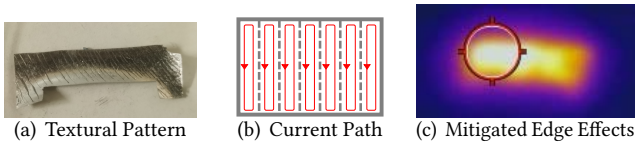

(a) Textural Pattern (b) Current Path (c) Mitigated Edge Effects

Figure 6: (a) A sample with textural liquid metal layer. (b) The path of induced eddy currents on the textural pattern. (c) The heat distribution of the textural layer shows that the edge effect is significantly mitigated, and the high temperature is uniformly distributed through the entire sample.

and thus degrades actuation performance. To combat the edge effect, WASER designs a fine-grained texture on the liquid metal layer instead of using a uniformly distributed composite. The key idea is to design thin laminates of liquid metal conductors on the conductive layer as shown in Fig. 6 (a). Using this approach, the eddy current will be induced within each lamination to mitigate the overall edge effects. Fig. 6 (b) shows the illustration of induced eddy current in our soft robot design and Fig. 6 (c) shows a much more uniform heat distribution, compared to the naïve design in Fig. 5 (a). We implement multiple textures of the conductive layer and evaluate their heating performance in Sec. 8.2.

6.2 Soft Robot Material and Fabrication

This section describes the material architecture and method for fabricating the WASER soft robot.

Primer on Materials for Soft Robots: Three types of materials have been widely used for soft robots, including ferrofluid, silicone elastomer, and electrothermal polymer. Ferrofluid is actuated through the use of changing magnetic fields [12], while silicon elastomer, which is toxic-free, easily accessible, and 3D-printable, is typically used for mechanical actuators such as robot palms and feet [73]. Electrothermal polymer, which is often fabricated in thin films or patches, is actuated via thermal stimulation, and is among the most popular materials for constructing soft robots due to its straightforward fabrication process and actuation mechanism [37, 42]. Liquid crystal elastomers (LCE) are a type of electrothermal polymer that exhibits significant shape changes at relatively low temperatures.

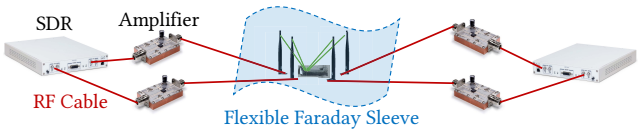

Figure 7: The WASER System Architecture.

Material Selection: To address the needs of a material architecture that can both be rapidly heated by wireless signals and exhibit repeatable actuation, we combine liquid crystal elastomers (LCE) with a thin film of mechanically deformable conductive material. LCE was selected for its ability to be a soft actuator that can contract and expand based on thermal stimuli. The LCE is fabricated in thin films (50 µm) that upon heating contract along one director and induce bending. To induce uniform contraction, polarized light is used to photopolymerize and align the mesogens along one director. For the conductive layer, a 3-6 µm of Silver and eutectic Gallium-Indium (EGaIn) liquid metal is coated on the surface of LCE. This thin layer does not impact mechanical performance due to its compliance and deformability.

Fabrication Method: The fabrication process has three steps: (1) LCE synthesis; (2) LCE photoalignment; (3) deposition of soft conductive films. Steps 1-2 are based on [34], and Step 3 is adapted from [58, 59].

7 IMPLEMENTATION

We build the first high-power beamforming platform for wireless heating applications that will be available to researchers in wireless, robotics, and material science. The hardware and documentation will be open-sourced upon paper acceptance. The platform is composed of RF chains, an enclosure that minimizes microwave leakage, and the WASER software.

RF Chain: The platform shown in Fig. 7 consists of multiple RF chains. Each RF chain has one USRP X310 as the signal generator. The USRP transmits 2.45 GHz signals with a maximum output power of 20.26 dBm that we verified using a spectrum analyzer. We then feed an RF LDMOS integrated power amplifier to the output of the USRP. We limit the output power of USRP to 20 dBm, which is the maximum input power of the amplifier. The amplifier provides a 29.7 dB linear power amplification to the 2.45 GHz band [45]. At the end of each RF chain, we have an omni-directional antenna that supports a 50 W maximum output [29]. During the experiments, we use four RF chains in total. The total transmitted power of WASER is limited to 20 W, but each chain is capable of providing 1 W - 14 W wireless power. When applying a 2.5 W total transmit power, WASER achieves the heating to 60 °C at 5 seconds (see Figure. 12 (c)).

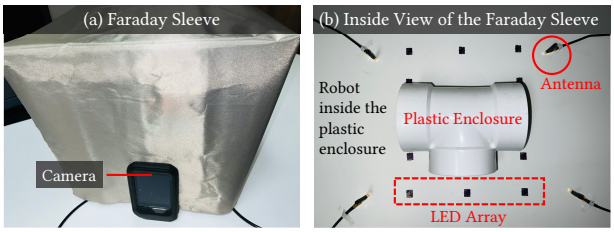

Figure 8: (a) The flexible Faraday enclosure. The camera views the LED harvesters inside of the enclosure via a small opening (6 mm wide) of the Faraday sleeve. (b) Inside view of the Faraday enclosure. The transmit antennas are in the non-line-of-sight from the soft robot, which is blocked by a plastic obstacle. 4 antennas and 10 LED harvesters are placed around the obstacle.

WASER System Setup: Fig. 8 shows an example of the system setup including the Faraday shield, a soft robot, a plastic obstacle, antennas, and an array of LED energy harvesters. The soft robot is in the non-line-of-sight, placed inside a plastic enclosure. The antennas are placed within the Faraday shield. A camera views the harvesters via a small opening (6 mm wide) of the Faraday shield to ensure minimal leakage [44]. The LED harvesters are placed around the obstacle (e.g., visible to the camera) but still within Faraday shielding. During evaluation, the LEDs are positioned on a circular arrangement with a radius of 55 mm, and an ELP 4mm Lens Prototype Camera ($53) [5] is utilized to capture the brightness of the LEDs. The movement area of the robot is confined to a region measuring 10 cm by 10 cm. The system's working distance is limited by the dimensions of the Faraday cage, which are 100 ft by 100 ft by 100 ft. Fig. 9 shows an illustration of the system geometry.

Flexible Faraday Sleeves: In order to ensure safety and avoid generating interference with existing Wi-Fi infrastructure, WASER uses a flexible and mobile Faraday sleeve to operate the actuation (see Fig. 8 (a)). The shielding sleeve is composed of double-layered EMF conductive fabrics [3]. It encloses the entire system shown in Fig. 8 (b). The volume of the entire RF shielded space can be scaled to 100 ft^3. Note that this flexible Faraday fabric provides 40 dB attenuation to the wireless signals at 2.45 GHz and prevents the microwave leakage in compliance with FCC regulations.

WASER Software: WASER runs its real-time channel inference and beamforming algorithm in C++ on a Linux laptop. WASER captures the LED responses using a low-cost camera. WASER implements the channel interpolation on MATLAB infused with electromagnetic and thermal modeling on CST studio. In addition to WASER's algorithm, we build a safety monitoring software that monitors the temperature of power

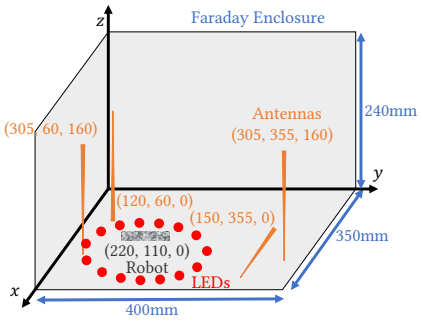

Figure 9: An illustration of the system geometry. The antennas (orange) are placed with various orientations to provide diverse spatial diversity. The soft robot (silver) is placed at $(220, 110, 0)$ and LEDs (red) surround the soft robot with a spacing of 25 mm.

amplifiers, the thermal distribution inside the cavity, and the microwave leakage outside the cavity.

Ground Truth and Baseline: We use a FLIR C5 Thermal Camera to measure the heat distribution, and use it as the ground truth to evaluate the heating resolution performance of WASER. We compare WASER against a four-antenna baseline system, that performs *phase sweeping*. The baseline does not perform accurate energy focusing as we described in Sec. 5. Instead, it sweeps a pre-generated set of low-power phase shifted signals to determine the beamforming vector for the robot actuation. Specifically, each antenna sweeps its phase from 0° to 360° in steps of 90°. We show how this system offers poorer heating performance. This baseline is denoted as *Sweeping* in our experimental results and graphs.

8 RESULTS

8.1 Channel Inference Accuracy

8.1.1 Probing Accuracy. WASER first probes the wireless channel information at multiple locations that LED harvesters are deployed as we describe in Sec. 5.2. In this section, we validate the channel probing accuracy on our testbed.

Method: We evaluate the accuracy of channel estimation of the LED harvesters using a four-antenna testbed and a single LED. We apply 16 channel probing for channel estimation and use another 16 probes to evaluate the accuracy.

Results: Fig. 10 (a) shows that our system converges to -4.5 dB error using seven probes, and maintains this with slight fluctuation. We note that the fluctuation can be caused by the impairments such as quantization errors and camera's non-linearity of LED brightness. In addition, we compare the WASER with a baseline that infers the channel without using LED harvesters. Specifically, we measure the channel by ray-tracing the radio environment inside the Faraday shield. The dotted red line in Fig. 10 (a) shows that the baseline

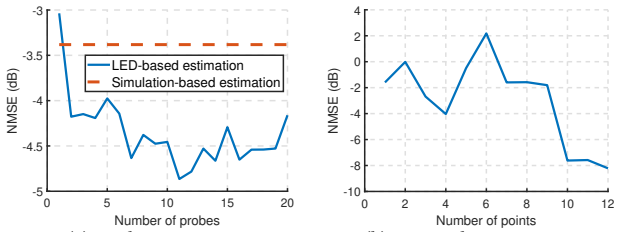

(a) Probing Accuracy (b) Interpolation Accuracy

Figure 10: (a) The normal mean squared error (NMSE) of WASER's channel probing converges to -4.5 dB after seven probes. The simulation-based baseline gives 1 dB higher error than WASER's. (b) The NMSE of channel interpolation converges to -7.9 dB using ten distributed LED harvesters.

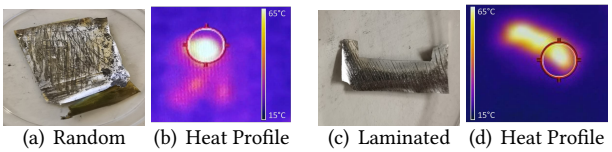

(a) Random (b) Heat Profile (c) Laminated (d) Heat Profile

Figure 11: WASER implements different textures on the conductive layer and evaluates their heat distributions. The thin lamination significantly mitigates the edge effects and achieves a uniform heat distribution.

approach has a 1 dB higher error compared to the WASER. This is because the real-world environment is multipath-rich – we cannot infer the accurate wireless channel by only relying on the geometry of the robot and RF antennas. Indeed, WASER needs to deploy an array of LED harvesters to learn the multipath components in the environment. We further note that the WASER's LED-based approach operates in real-time and is generalizable to various environment, while the ray-tracing baseline is time-consuming.

8.1.2 Interpolation Accuracy. Once WASER probes the channel of the LED array, WASER can interpolate the wireless channel of the robot. We describe the algorithm in Sec. 5.3.

Method: We evaluate the accuracy of channel interpolation using a single antenna and thirteen distributed LED harvesters with a 50 mm spacing, among which twelve LEDs are used for providing interpolation data (obtained from channel probing) and one LED is used for evaluation. We initialize the optimization informed by our simulation.

Results: As in Fig. 10 (b), the channel interpolation error decreases to -7.9 dB using ten distributed LED harvesters. Overall, WASER achieves a higher accuracy in channel interpolation with a higher number of deployed LED harvesters.

8.2 Impact of Liquid Metal Patterns

Method: This section evaluates the heating performance on different textural designs of the liquid metal layer of the soft robot. The goal of designing a textural conductive layer instead of a uniform one is to combat edge effects (see Fig. 6 (b)) and improve the heating distribution over the soft robot. Specifically, WASER implements two patterns of the textural conductive layer: random texture and uniformly thin laminates. Different textures are applied to the liquid metal during the material fabrication process. We deploy the two samples shown in Fig 11 (a) and (c) at the same location and compare their heat distribution when applying a single-antenna 12.5 W power source at 2.4 GHz.

Results: Fig. 11 (b) and (d) show the heat distribution of the random texture and the thinly laminated texture respectively. We observe the thinly laminated texture achieves a uniform heat distribution across the entire sample. However, the heat distribution of the random textural sample is random and one of the corners is overheated than other parts. We note that this is because the induced Eddy currents across the random textural surface is non-uniform. Therefore, we use the thinly laminated texture as our final design.

8.3 Impact of Number of Antennas

We evaluate WASER's heating performance as we vary the number of distributed antennas when the total transmitted power remains the same (2.5 Watts).

Method: We deploy up to four antennas. Fig. 9 shows the location and orientation of the antennas. We consider various locations and orientations of the soft robot in both line-of-sight (LoS) and non-line-of-sight (NLoS). We compare our algorithm with two baselines: (1) phase *sweeping* as we described in Sec. 7; (2) a single-antenna setup without any energy focusing. Across all experiments, the total transmit power remains 2.5 W, and each antenna transmits the same power. We note that the distance between the robot and the closest antenna is longer than 12 cm, but shorter than 22 cm.

Results: Fig. 12 (a) shows the soft robot's average temperature across various locations with respect to increasing the time of actuation when using various number of antennas. For the single-antenna baseline, we observe that the temperature barely increases after 10 seconds as the heating effect and temperature dissipation reach a balance. Indeed, WASER outperforms the single-antenna and the *Sweeping* baseline by relying on its beamforming algorithm which can precisely focus the energy on the robot. As the number of antennas increases, WASER achieves a higher temperature at increasing speed. Specifically, WASER heats the robot to 60 °C taking 11 seconds on average considering various locations, but the phase sweeping baseline takes 20 seconds on average to reach 60 °C. But for all cases, the speed of temperature increase decreases with time until equilibrium. Fig. 12 (b) shows the bar plot of the soft robot's temperature at 5 seconds of heating. We note that the median of the temperature

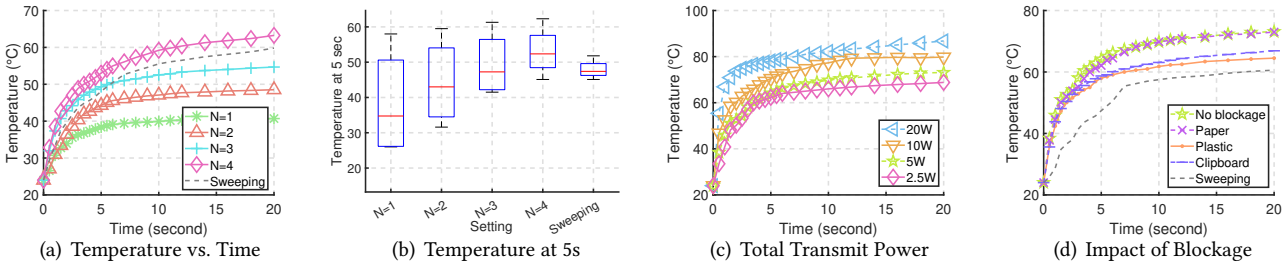

(a) Temperature vs. Time (b) Temperature at 5s (c) Total Transmit Power (d) Impact of Blockage

Figure 12: (a&b) WASER's multi-antenna beamforming approach achieves a better performance in the speed of heating soft robots as the number of antennas increases, and outperforms the four-antenna baseline considering various locations of the robot in both LoS and NLoS. (c) WASER achieves the heating to 60 °C at 5 seconds when applying 2.5 W (the typical transmit power of a Wi-Fi repeater [4]) to the soft robot at the coordinates (220, 110, 0) shown in Fig. 9. This is an 8× improvement in the speed of actuation compared to the prior work [69] which uses a hundred-Watt transmit power. (d) WASER is resilient to various materials of blockage.

increases and the variance of the temperature decreases as WASER uses more distributed antennas. Overall, WASER's performance in heating increases by 50% and 8% compared to the single-antenna and the *Sweeping* baseline respectively.

8.4 Heating vs. Total Transmitted Power

Method: We evaluate the impact of total transmitted power on the temperature using the four-antenna setup. Specifically, we apply the 2.5 W, 5 W, 10 W, and 20 W total transmitted power respectively. Here, we keep the soft robot at the same location which is at coordinate (220, 110, 0) shown in Fig. 9.

Results: Fig. 12 (c) shows the temperature vs. the increase in time under different total transmitted power. We observe that WASER achieves heating the soft robot to 60 °C at 1.5 seconds when applying 20 W from four antennas – a 27 times improvement compared to prior work [69]. Even using 2.5 W which is the typical transmit power of a long-range Wi-Fi repeater [4], WASER achieves 60 °C at around 5 seconds. We note that even though we apply a high transmitted power at the transmitter, the microwave leakage from our Faraday sleeve is well below the FCC regulation.

8.5 Impact of Blockage

Method: We evaluate the impact of blockage on the heating performance when the robot is in the non-line-of-sight from the beamforming platform. Specifically, we deploy different types of blockage such as plastic and wood to enclose the robot. Across the experiments, we use our four-antenna setup with a 5 W total transmitted power.

Results: Fig. 12 (d) shows the temperature of the soft robot being heated under various types of blockage. We observe that the paper occlusion has a minimal impact in our system performance, which increases the time to reach 60 °C by about 0.5 seconds compared to the line-of-sight setting.

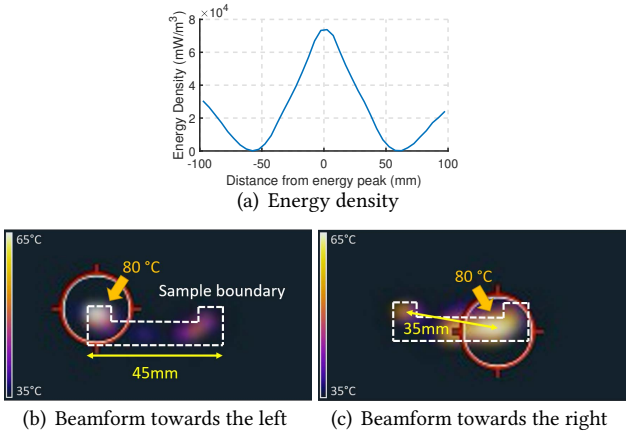

(a) Energy density (b) Beamform towards the left (c) Beamform towards the right

Figure 13: (a) The theoretical heating resolution of WASER. We define the heating resolution as the distance that the energy density attenuates 3 dB from the peak. (b&c) We evaluate the heating resolution of WASER by focusing the energy towards the two ends of a 45 mm long soft robot. We show a 17.8 mm heating resolution on average.

While the time to reach 60 °C under plastic and wooden blockage increases by 2 and 3 seconds respectively compared to the LoS setting, WASER's beamforming approach outperforms the phase sweeping baseline, improving the time to reach 60 °C by at least 9 seconds, even if the soft robot is in non-line-of-sight.

8.6 Heating Resolution

We evaluate the heating resolution by beamforming at one side of the soft robot, while nulling the energy at the other side. Note that the *Sweeping* baseline is not capable of achieving a high heating resolution since it only provides rough spatial resolution. Fig. 13 (a) shows the simulated energy density that WASER can achieve using a four-antenna setup.

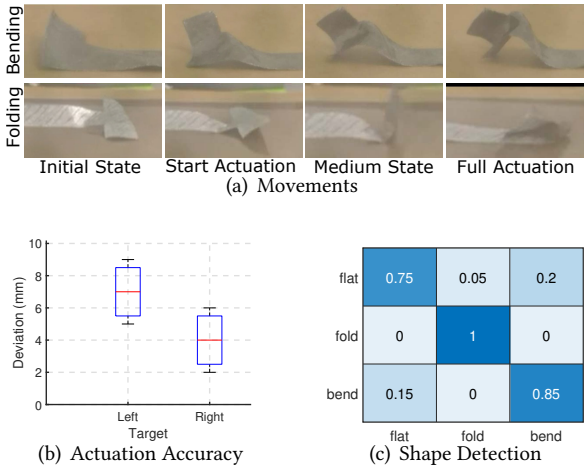

(a) Movements (b) Actuation Accuracy (c) Shape Detection

Figure 14: (a) Snapshots of WASER Movements. (b) Accuracy of Shape Changes. (c) WASER can detect the various shape changes when the robot is actuated.

The simulated heat resolution is around 20 mm. We evaluate the heating resolution by beamforming at two ends of the sample shown in Fig. 6 (a). Fig. 13 shows the heat maps filmed by a thermal camera with the two beamforming vectors. Fig. 13 (b) shows that the left part is heated to 80 °C, while the rest remains below 40 °C. Fig. 13 (c) shows the right part is heated to 80 °C, while the left is still under 40 °C. Overall, WASER achieves a 17.8 mm heating resolution. We note this minor variations between the actual and simulated heating resolution is due to differences in the material properties between the fabricated and simulated robot.

8.7 Shape Morphing

We present two key proof-of-concept actuation examples.

Bending: The robot is designed to bend when particular parts are actuated. The robot is flat before it is beamed energy. In this experiment, we beam the energy towards the left side of the robot and induce a complete bending downwards to support its own weight.

Folding: We demonstrate a folding motion shown in Fig. 14 (a). The shape changing capability (e.g., folding) is embedded into the soft robot during its fabrication process. Further information on the fabrication process of these samples is given in Sec. 6.2.

Accuracy of Shape Changes: The ability to accurately move the soft robot to exhibit desired shape changes is crucial. We evaluate the accuracy in inducing desired shape changes of WASER's soft robot. Specifically, we beam maximized energy to the leftmost and rightmost part of the soft robot which is expected to exhibit two shape changes – the leftmost and the rightmost part flipping downwards respectively. In the experiments, we measure the ground truth shape changes of the soft robot using a camera. We then measure the deviation (Euclidean distance) between actual and desired maximum hotspot locations. Fig. 14 (b) shows our results. We demonstrate that the soft robot exhibits an average of 7 mm and 4 mm deviation from the desired shape change for the leftmost and rightmost movements respectively. We note that this deviation can be further improved through reducing fabrication imperfections of the soft robot.

Shape Change Detection: WASER can detect the shape change of the robot being actuated so that WASER can potentially apply a series of actuation to enable continuous shape changes. Specifically, WASER detects the movement by leveraging four deployed 2.4GHz LEDs around the sample. We use a data-driven approach to learn the LED responses when three types of shape changes are actuated: flat, fold and bend. WASER then evaluates the accuracy of the shape detection by applying 20 times of actuation for each type of shape change. Fig. 14 (c) shows that the our system achieves a 0.75, 1.0, and 0.85 accuracy in classifying the flat, fold, and bend status, respectively.

9 DISCUSSION AND LIMITATIONS

Path Loss and EM-to-Heat Efficiency: The path loss and the EM-to-heat energy conversion efficiency of the material are the two fundamental factors that limit the system's total transmit power. In terms of wireless transmission, the implementation of highly directional antennas on either the robot or the transmitters can effectively decrease the path loss. On the material side, enhancing the energy conversion efficiency can be achieved by incorporating higher conductive materials, such as gold, in place of the EGaIN liquid metal used for the conductive layer, thereby increasing the strength of the eddy current generated throughout the robot.

Faraday Shields: We note that the maximum transmit power of WASER is 20 Watts (43 dBm) – the typical transmit power of a 4G cellular antenna [6]. Received power further decays by 40 dB even at distances of about 1 meter from WASER. However, in the interest of safety, WASER is best deployed within an RF enclosure to ensure minimal RF leakage. Instead of using a bulky Faraday cage, WASER builds a light-weight Faraday sleeve composed of flexible EMI shielding fabrics [3] as shown in Fig. 8. Such flexible materials provide ~40 dB attenuation to the RF signals at 2.45 GHz. We believe this flexible Faraday sleeve makes the whole system less bulky and lower cost. The overall weight of this Faraday sleeve is less than 100 grams, which is much less bulky and more mobile than other traditional Faraday cages.

To Eliminate Faraday Shields: WASER's use of a Faraday shield can be eliminated by reducing the total transmit power.

We've demonstrated that WASER is able to actuate the soft robot with a very low transmit power (e.g., 2.5 W) which is the typical transmit power of a long-range Wi-Fi repeater. We believe a reduced transmit power (e.g., 1 Watt) without sacrificing the capability of actuating wireless electronics-free soft robots can be achieved by future improvements from multiple perspectives: (1) *Materials:* creating LCE materials be capable of performing shape changes at a lower temperature; using a higher conductive material such as gold to induce a stronger eddy current throughout the robot. (2) *Higher Frequency:* Moving to a much higher frequency such as 60 GHz millimeter wave can significantly reduce the side lobe energy leakage and enable better energy focus because of a much shorter wavelength ($\sim$ 5 mm) than 2.4 GHz — using a much less transmit power but beaming more focused RF energy to power the soft robot. We believe WASER is a starting point for a rich space for future exploration.

More Complex Movements: In this paper, we present relatively simple shape changes and movements of parts of the soft robot. However, a series of more complex moves can be performed based on the simple moves. Specifically, WASER applies a series of beamforming vectors to induce the continuous movements. For example with alternating bending and folding, a soft robot may be able to perform crawl-like movements. In addition, motion in reverse require the robot cooling down. This may take time for our current implementation, but researchers in soft robots propose innovations in reducing the cooling time [28]. More complex movements can be further improved by augmenting the shape morphing capability of the soft robot itself [19, 70]. Doing so does require more advanced mechanical design of the soft robot, but we believe that the WASER platform is a natural complement to such research in soft robotics.

The Location of the Soft Robot: WASER assumes that the location of the soft robot is known, although its shape changes under heating can be inferred as shown in Sec. 8.7. Potential methods to localize and sense the actual shape change of the electronics-free soft robot could leverage wireless localization techniques based on acoustics or mmWave Radar – we leave this for future exploration.

Potential Use-cases and Their Required Future Efforts: The actuation platform of WASER itself can serve as an important building block to enable future research in soft robotics, material science, and wireless systems. The electronics-free soft robot wirelessly actuated by WASER has wide-ranging potential use-cases. Here, we list some examples that could be built and evaluated in follow-up work.
(a) **Chemical Release:** For example, a soft robot in an inner cavity can be remotely controlled from an external RF source to change its state of shape deformation and then perform on-demand release of chemicals (e.g., disinfectants) stored within the cavity (e.g. a robot within a plastic pipe or enclosure). This scenario necessitates the development of an internal cavity within the soft robot's structure. Furthermore, the soft robot should be able to move with the payloads.
(b) **Sensing in Enclosed Spaces:** WASER robots could be instrumented with passive sensing platforms (e.g. pH paper) within enclosed spaces (e.g. pipes/containers) that can be exposed as needed for sensing with external actuation. The implementation of this use case entails the creation of an internal compartment within the soft robot to accommodate the sensing platform and the development of a flexible LCE-made cover that can only be actuated by the WASER platform. Upon actuation, the sensing platform (e.g., pH paper) becomes accessible for environmental sensing.
(c) **Ubicomp/HCI Use-cases:** We believe that wirelessly controlled mobility of soft robots allows for new forms of mobile and ubiquitous systems. We also note that soft devices and robots themselves are an emerging novel platform used in various HCI and ubiquitous applications, for example, these soft surfaces are promising to serve as a wearable platform for interfaces and adaptive environments. In addition to that, WASER soft robots can be utilized for innovative sensing applications, such as deformation sensing and stretch sensing. The major concerns are the transmit power of the system and the heat induced on the robot but we envision that those limitations can be further explored by future efforts such as new materials and directional transmitters. We leave the evaluation of these use-cases to future work.

10 CONCLUSION

This paper presents WASER, a solution that uses highly-controlled microwave radiation to control the movement and shape of elastomer-based soft robotic platforms. WASER achieves this through innovations in wireless systems and material science. On the wireless front, WASER develops a blind beamforming solution that rapidly focuses energy at desired points on the robot to heat and induce shape changes, without electronics on the robot. On the materials front, we develop novel material designs that improve the heating efficiency of the platform without inducing high bulk and rigidity. WASER is fully implemented and evaluated on soft robotic platforms. We believe there is rich scope for future work that builds on WASER, particularly in exploring diverse use-cases and applications of wirelessly actuated soft robotics for industrial and aerospace applications.

Acknowledgments: We thank NSF (2030154, 2106921, 2007786, 1942902, 2111751), ARL, DARPA-TRIAD and MFI for their support.

REFERENCES

[1] Abu-Saleem, M., Zhuge, Y., Hassanli, R., Ellis, M., Rahman, M. M., and Levett, P. Microwave radiation treatment to improve the strength of recycled plastic aggregate concrete. *Case Studies in Construction Materials 15* (2021), e00728.

[2] Ahmed, I., Khammari, H., Shahid, A., Musa, A., Kim, K. S., De Poorter, E., and Moerman, I. A survey on hybrid beamforming techniques in 5g: Architecture and system model perspectives. *IEEE Communications Surveys & Tutorials 20*, 4 (2018), 3060–3097.

[3] Amazon. Faraday fabric. https://www.amazon.com/dp/B0875V2F7M?ref_=cm_sw_r_cp_ud_dp_VBFCZDPK98VWAM2W3S1Z, 03 2022. (Accessed on 03/15/2022).

[4] Amazon. Sunhans sh-2500 2500mw wireless signal repeater 33dbm wifi signal booster 2.5w. https://www.amazon.com/Sunhans-Sh-2500-Wireless-Repeater-Booster/dp/B00HJ1NQLS, 01 2022. (Accessed on 01/15/2022).

[5] Amazon. Elp usb camera. https://www.amazon.com/ELP-4mm-Lens-Prototype-Camera/dp/B01N3QO9JW/ref=as_li_ss_tl?s=photo&ie=UTF8&qid=1483961121&sr=1-12&keywords=ov2710&th=1&linkCode=ll1&tag=tuio0d-20&linkId=3c6f0cabb55d67c867f914a4b9404c08, 02 2023. (Accessed on 02/10/2023).

[6] Behnke, K. Is this anything to worry about? 5g health issues explained. https://www.grandmetric.com/2019/03/26/5g-health-issues-explained/, 01 2022. (Accessed on 01/15/2022).

[7] Boothby, J. M., Gagnon, J. C., McDowell, E., Van Volkenburg, T., Currano, L., and Xia, Z. An Untethered Soft Robot Based on Liquid Crystal Elastomers. *Soft Robotics 00*, 00 (2021), 1–9.

[8] Candes, E. J., Strohmer, T., and Voroninski, V. Phaselift: Exact and stable signal recovery from magnitude measurements via convex programming. *Communications on Pure and Applied Mathematics 66*, 8 (2013), 1241–1274.

[9] Chabalko, M. J., and Sample, A. P. Three-dimensional charging via multimode resonant cavity enabled wireless power transfer. *IEEE Transactions on Power Electronics 30*, 11 (2015), 6163–6173.

[10] de la Hoz, A., Díaz-Ortiz, A., and Prieto, P. Microwave-assisted green organic synthesis.

[11] Design, C. Successful induction heating of rcs billets.

[12] Fan, X., Dong, X., Karacakol, A. C., Xie, H., and Sitti, M. Reconfigurable multifunctional ferrofluid droplet robots. *Proceedings of the National Academy of Sciences 117*, 45 (2020), 27916–27926.

[13] Fan, X., Shangguan, L., Howard, R., Zhang, Y., Peng, Y., Xiong, J., Ma, Y., and Li, X.-Y. Towards flexible wireless charging for medical implants using distributed antenna system. In *Proceedings of the 26th Annual International Conference on Mobile Computing and Networking* (New York, NY, USA, 2020), MobiCom '20, Association for Computing Machinery.

[14] Ford, M. J., Ambulo, C. P., Kent, T. A., Markvicka, E. J., Pan, C., Malen, J., Ware, T. H., and Majidi, C. A multifunctional shape-morphing elastomer with liquid metal inclusions. *Proceedings of the National Academy of Sciences 116*, 43 (2019), 21438–21444.

[15] Gelebart, A. H., Jan Mulder, D., Varga, M., Konya, A., Vantomme, G., Meijer, E., Selinger, R. L., and Broer, D. J. Making waves in a photoactive polymer film. *Nature 546*, 7660 (2017), 632–636.

[16] Gertsman, S., Agarwal, A., O'Hearn, K., Webster, R., Tsampalieros, A., Barrowman, N., Sampson, M., Sikora, L., Staykov, E., Ng, R., Gibson, J., Dinh, T., Agyei, K., Chamberlain, G., and McNally, J. Microwave- and heat-based decontamination of n95 filtering facepiece respirators: a systematic review. *Journal of Hospital Infection 106*, 3 (2020), 536–553.

[17] Gupta, M., and Leong, E. W. W. *Microwaves and metals*. John Wiley & Sons, 2008.

[18] Guru, B. S., and Hiziroglu, H. R. *Electromagnetic field theory fundamentals*. Cambridge university press, 2009.

[19] Hawkes, E., An, B., Benbernou, N. M., Tanaka, H., Kim, S., Demaine, E. D., Rus, D., and Wood, R. J. Programmable matter by folding. *Proceedings of the National Academy of Sciences 107*, 28 (2010), 12441–12445.

[20] He, Q., Wang, Z., Wang, Y., Minori, A., Tolley, M. T., and Cai, S. Electrically controlled liquid crystal elastomer–based soft tubular actuator with multimodal actuation. *Science advances 5*, 10 (2019), eaax5746.

[21] Hines, L., Petersen, K., Lum, G. Z., and Sitti, M. Soft actuators for small-scale robotics. *Advanced materials 29*, 13 (2017), 1603483.

[22] Hong, C., Ren, Z., Wang, C., Li, M., Wu, Y., Tang, D., Hu, W., and Sitti, M. Magnetically actuated gearbox for the wireless control of millimeter-scale robots. *Science Robotics 7*, 69 (2022), eabo4401.

[23] Hossan, M. R., Byun, D., and Dutta, P. Analysis of microwave heating for cylindrical shaped objects. *International Journal of Heat and Mass Transfer 53*, 23-24 (2010), 5129–5138.

[24] Hu, J., Kuang, Z.-Y., Tao, L., Huang, Y.-F., Wang, Q., Xie, H.-L., Yin, J.-R., and Chen, E.-Q. Programmable 3d shape-change liquid crystalline elastomer based on a vertically aligned monodomain with cross-link gradient. *ACS Applied Materials & Interfaces 11*, 51 (2019), 48393–48401.

[25] Hu, W., Lum, G. Z., Mastrangeli, M., and Sitti, M. Small-scale soft-bodied robot with multimodal locomotion. *Nature 554*, 7690 (2018), 81–85.

[26] Huang, C., Lv, J.-a., Tian, X., Wang, Y., Yu, Y., and Liu, J. Miniaturized swimming soft robot with complex movement actuated and controlled by remote light signals. *Scientific reports 5*, 1 (2015), 1–8.

[27] Huang, X., Ford, M., Patterson, Z. J., Zarepoor, M., Pan, C., and Majidi, C. Shape memory materials for electrically-powered soft machines. *Journal of Materials Chemistry B 8*, 21 (2020), 4539–4551.

[28] Huang, X., Ren, Z., and Majidi, C. Soft thermal actuators with embedded liquid metal microdroplets for improved heat management. In *2020 3rd IEEE International Conference on Soft Robotics (RoboSoft)* (2020), pp. 367–372.

[29] Inc., L. C. Rf ant 2.4ghz whip str sma male. https://www.digikey.com/en/products/detail/laird-connectivity-inc/WXE2400SM/2392260, 01 2022. (Accessed on 01/15/2022).

[30] Jamin, T., Py, C., and Falcon, E. Instability of the origami of a ferrofluid drop in a magnetic field. *Physical Review Letters 107*, 20 (2011), 204503.

[31] Jin, H., Wang, J., Kumar, S., and Hong, J. Software-defined cooking using a microwave oven. In *The 25th Annual International Conference on Mobile Computing and Networking* (New York, NY, USA, 2019), MobiCom '19, Association for Computing Machinery.

[32] Kent, T. A., Ford, M. J., Markvicka, E. J., and Majidi, C. Soft actuators using liquid crystal elastomers with encapsulated liquid metal joule heaters. *Multifunctional Materials 3*, 2 (jun 2020), 025003.

[33] Kim, H., Ahn, S.-k., Mackie, D. M., Kwon, J., Kim, S. H., Choi, C., Moon, Y. H., Lee, H. B., and Ko, S. H. Shape morphing smart 3d actuator materials for micro soft robot. *Materials Today 41* (2020), 243–269.

[34] Kim, H., Gibson, J., Maeng, J., Saed, M. O., Pimentel, K., Rihani, R. T., Pancrazio, J. J., Georgakopoulos, S. V., and Ware, T. H. Responsive, 3d electronics enabled by liquid crystal elastomer substrates. *ACS applied materials & interfaces 11*, 21 (2019), 19506–19513.

[35] Kularatne, R. S., Kim, H., Boothby, J. M., and Ware, T. H. Liquid crystal elastomer actuators: Synthesis, alignment, and applications. *Journal of Polymer Science Part B: Polymer Physics 55*, 5 (mar 2017), 395–411.

[36] Kumar, S., Cifuentes, D., Gollakota, S., and Katabi, D. Bringing cross-layer mimo to today's wireless lans. In *Proceedings of the ACM*

SIGCOMM 2013 conference on SIGCOMM (2013), pp. 387–398.

[37] Lee, H., Kim, H., Ha, I., Jung, J., Won, P., Cho, H., Yeo, J., Hong, S., Han, S., Kwon, J., et al. Directional shape morphing transparent walking soft robot. *Soft Robotics 6*, 6 (2019), 760–767.

[38] Liu, X., Kim, S.-K., and Wang, X. Thermomechanical liquid crystalline elastomer capillaries with biomimetic peristaltic crawling function. *Journal of Materials Chemistry B 4*, 45 (2016), 7293–7302.

[39] Ma, S., Li, X., Huang, S., Hu, J., and Yu, H. A light-activated polymer composite enables on-demand photocontrolled motion: Transportation at the liquid/air interface. *Angewandte Chemie 131*, 9 (2019), 2681–2685.

[40] Ma, Y., Luo, Z., Steiger, C., Traverso, G., and Adib, F. Enabling deep-tissue networking for miniature medical devices. In *Proceedings of the 2018 Conference of the ACM Special Interest Group on Data Communication* (2018), pp. 417–431.

[41] Metageek. Wi-fi signal strength basics. https://www.metageek.com/training/resources/wifi-signal-strength-basics/, 01 2022. (Accessed on 01/15/2022).

[42] Miriyev, A., Stack, K., and Lipson, H. Soft material for soft actuators. *Nature communications 8*, 1 (2017), 596.

[43] Molex. Antenna omni-directional 3.3dbi gain 2483.5mhz. https://www.arrow.com/en/products/0479480001/molex, 01 2022. (Accessed on 01/15/2022).

[44] Murugan, J. T., Kumar, T. S., Salil, P., and Venkatesh, C. Dual frequency selective transparent front doors for microwave oven with different opening areas. *progress in electromagnetics research letters 52* (2015), 11–16.

[45] NXP. Rf ldmos integrated power amplifier. https://www.nxp.com/docs/en/data-sheet/MHT2012N.pdf, 07 2018.

[46] Ohm, C., Brehmer, M., and Zentel, R. Liquid crystalline elastomers as actuators and sensors. *Advanced materials 22*, 31 (2010), 3366–3387.

[47] Ozkan, I. A., Akbudak, B., and Akbudak, N. Microwave drying characteristics of spinach. *Journal of food engineering 78*, 2 (2007), 577–583.

[48] Palazoğlu, T. K., and Miran, W. Experimental comparison of microwave and radio frequency tempering of frozen block of shrimp. *Innovative Food Science & Emerging Technologies 41* (2017), 292–300.

[49] Rahul, H. S., Kumar, S., and Katabi, D. Jmb: scaling wireless capacity with user demands. *ACM SIGCOMM Computer Communication Review 42*, 4 (2012), 235–246.

[50] Rich, S. I., Wood, R. J., and Majidi, C. Untethered soft robotics. *Nature Electronics 1*, 2 (2018), 102–112.

[51] Rogóż, M., Dradrach, K., Xuan, C., and Wasylczyk, P. A millimeter-scale snail robot based on a light-powered liquid crystal elastomer continuous actuator. *Macromolecular rapid communications 40*, 16 (2019), 1900279.

[52] Rogóż, M., Zeng, H., Xuan, C., Wiersma, D. S., and Wasylczyk, P. Light-driven soft robot mimics caterpillar locomotion in natural scale. *Advanced Optical Materials 4*, 11 (2016), 1689–1694.

[53] Roh, W., Seol, J.-Y., Park, J., Lee, B., Lee, J., Kim, Y., Cho, J., Cheun, K., and Aryanfar, F. Millimeter-wave beamforming as an enabling technology for 5g cellular communications: Theoretical feasibility and prototype results. *IEEE communications magazine 52*, 2 (2014), 106–113.

[54] Rus, D., and Tolley, M. T. Design, fabrication and control of soft robots. *Nature 521*, 7553 (2015), 467–475.

[55] Sasatani, T., Sample, A. P., and Kawahara, Y. Room-scale magneto-quasistatic wireless power transfer using a cavity-based multimode resonator. *Nature Electronics 4*, 9 (Sep 2021), 689–697.

[56] Sasatani, T., Yang, C. J., Chabalko, M. J., Kawahara, Y., and Sample, A. P. Room-wide wireless charging and load-modulation communication via quasistatic cavity resonance. *Proc. ACM Interact. Mob. Wearable Ubiquitous Technol. 2*, 4 (Dec. 2018).

[57] Semiconductor, R. Sml-p11utt86r - rohm semiconductor. https://fscdn.rohm.com/en/products/databook/datasheet/opto/led/chip_mono/sml-p11-e.pdf, 01 2022. (Accessed on 01/15/2022).

[58] Silva, A. F., Paisana, H., Fernandes, T., Góis, J., Serra, A., Coelho, J. F., de Almeida, A. T., Majidi, C., and Tavakoli, M. High resolution soft and stretchable circuits with pva/liquid-metal mediated printing. *Advanced Materials Technologies 5*, 9 (2020), 2000343.

[59] Tavakoli, M., Malakooti, M. H., Paisana, H., Ohm, Y., Green Marques, D., Alhais Lopes, P., Piedade, A. P., de Almeida, A. T., and Majidi, C. Egain-assisted room-temperature sintering of silver nanoparticles for stretchable, inkjet-printed, thin-film electronics. *Advanced Materials 30*, 29 (2018), 1801852.

[60] Terentjev, E. M. Liquid-crystalline elastomers. *Journal of Physics: Condensed Matter 11*, 24 (1999), R239.

[61] Tian, H., Wang, Z., Chen, Y., Shao, J., Gao, T., and Cai, S. Polydopamine-coated main-chain liquid crystal elastomer as optically driven artificial muscle. *ACS applied materials & interfaces 10*, 9 (2018), 8307–8316.

[62] Tolley, M. T., Shepherd, R. F., Mosadegh, B., Galloway, K. C., Wehner, M., Karpelson, M., Wood, R. J., and Whitesides, G. M. A resilient, untethered soft robot.

[63] Trimmer, B. A., Lin, H.-T., Baryshyan, A., Leisk, G. G., and Kaplan, D. L. Towards a biomorphic soft robot: design constraints and solutions. In *2012 4th IEEE RAS & EMBS International Conference on Biomedical Robotics and Biomechatronics (BioRob)* (2012), IEEE, pp. 599–605.

[64] Van Veen, B. D., and Buckley, K. M. Beamforming: A versatile approach to spatial filtering. *IEEE assp magazine 5*, 2 (1988), 4–24.

[65] Wallin, T., Pikul, J., and Shepherd, R. 3d printing of soft robotic systems. *Nature Reviews Materials 3*, 6 (2018), 84–100.

[66] Wang, C., Sim, K., Chen, J., Kim, H., Rao, Z., Li, Y., Chen, W., Song, J., Verduzco, R., and Yu, C. Soft ultrathin electronics innervated adaptive fully soft robots. *Advanced Materials 30*, 13 (2018), 1706695.

[67] Wang, J., Zhang, J., Li, K., Pan, C., Majidi, C., and Kumar, S. Locating everyday objects using nfc textiles. In *Proceedings of the 20th International Conference on Information Processing in Sensor Networks (co-located with CPS-IoT Week 2021)* (2021), pp. 15–30.

[68] Wang, J., Zhang, J., Saha, R., Jin, H., and Kumar, S. Pushing the range limits of commercial passive {RFIDs}. In *16th USENIX Symposium on Networked Systems Design and Implementation (NSDI 19)* (2019), pp. 301–316.

[69] Wang, X., Wang, Y., Wang, X., Niu, H., Ridi, B., Shu, J., Fang, X., Li, C., Wang, B., Gao, Y., et al. A study of the microwave actuation of a liquid crystalline elastomer. *Soft Matter 16*, 31 (2020), 7332–7341.

[70] Ware, T. H., McConney, M. E., Wie, J. J., Tondiglia, V. P., and White, T. J. Voxelated liquid crystal elastomers. *Science 347*, 6225 (feb 2015), 982–984.

[71] Wehner, M., Truby, R. L., Fitzgerald, D. J., Mosadegh, B., Whitesides, G. M., Lewis, J. A., and Wood, R. J. An integrated design and fabrication strategy for entirely soft, autonomous robots. *nature 536*, 7617 (2016), 451–455.

[72] Yakacki, C., Saed, M., Nair, D., Gong, T., Reed, S., and Bowman, C. Tailorable and programmable liquid-crystalline elastomers using a two-stage thiol–acrylate reaction. *Rsc Advances 5*, 25 (2015), 18997–19001.

[73] Yirmibesoglu, O. D., Morrow, J., Walker, S., Gosrich, W., Cañizares, R., Kim, H., Daalkhaijav, U., Fleming, C., Branyan, C., and Menguc, Y. Direct 3d printing of silicone elastomer soft robots and their performance comparison with molded counterparts. In *2018 IEEE International Conference on Soft Robotics (RoboSoft)* (2018), pp. 295–302.

[74] Young, S., Graves, D., Rohrer, M., and Bulard, R. Microwave sterilization of nitrous oxide nasal hoods contaminated with virus. *Oral Surgery, Oral Medicine, Oral Pathology 60*, 6 (1985), 581–585.

[75] Zadan, M., Patel, D. K., Sabelhaus, A. P., Liao, J., Wertz, A., Yao, L., and Majidi, C. Liquid crystal elastomer with integrated soft thermoelectrics for shape memory actuation and energy harvesting. *Advanced Materials* (2022), 2200857.

[76] Zuo, B., Wang, M., Lin, B.-P., and Yang, H. Visible and infrared three-wavelength modulated multi-directional actuators. *Nature communications 10*, 1 (2019), 1–11.